Relationship between Regiospecificity and Type of Stereospecificity in Propene Polymerization with Zirconocene-Based Catalysts[1]

Gaetano Guerra,*,† Pasquale Longo,† Luigi Cavallo,‡ Paolo Corradini,‡ and Luigi Resconi§

Contribution from the Dipartimento di Chimica, Università di Salerno, I-84081 Baronissi (Salerno), Italy, Dipartimento di Chimica, Università di Napoli Federico II, Via Mezzocannone 4, I-80134, Naples, Italy, and Montell Polyolefins, G. Natta Research Center, P. le G. Donegani 12, I-44100, Ferrara, Italy

Received December 2, 1996[⊗]

Abstract: The microstructures of polypropenes produced with several zirconocene-based catalyst systems are compared, to verify the possible correlation between the type of stereospecificity and the amount of regioirregularities. It is confirmed that, while syndiospecific and aspecific zirconocenes are highly regiospecific, isospecific systems produce substantial amounts of regioirregular monomeric units. The amount of these secondary units strongly depends on the nature of the π-ligands and on the type of the bridge connecting them. Molecular mechanics calculations are reported, indicating that the intermediates which are energetically suitable for the secondary and primary insertions, for isospecific or syndiospecific complexes, coordinate monomer enantiofaces of the opposite or the same chirality, respectively. This difference accounts for the lower regiospecificity of the isospecific catalytic complexes, assuming that the energy barrier for the rotation of the coordinated monomer around the metal−olefin bond, between the orientations suitable for the primary and secondary insertions is lower than (or comparable to) the activation energy for secondary monomer insertion.

Introduction

Ewen[2] and Kaminsky[3] showed that the homogeneous catalyst systems composed of Brintzinger's[4] *rac*-ethylenebis(1-indenyl)-$MtCl_2$ or *rac*-ethylenebis(4,5,6,7-tetrahydro-1-indenyl)$MtCl_2$ (Mt = Ti, Zr, Hf) and methylalumoxane (MAO) produce isotactic polypropene (iPP) by enantiomorphic site control. The mechanism of isospecific propene polymerization with chiral (C_2 as well as C_1 symmetric) group 4A metallocene catalysts has been rationalized by molecular mechanics analyses on monometallic single-center catalysts by some of us[5] and by others.[6]

Contrary to iPP samples produced by catalytic systems based on titanocenes, which are always highly regioregular,[2,7] the iPP samples from catalytic systems based on zirconocenes and hafnocenes contain isolated secondary (2,1 insertions, up to 3%) propene units and isolated 3,1 propene units (arising from the unimolecular isomerization of 2,1 units, 0-5%) in the isotactic sequences of primary propene insertions.[8] The relative amounts of these regiodefects are highly dependent on the metallocene and the polymerization conditions employed.[8] Regioirregularities have been observed not only for isospecific catalytic systems based on C_2-symmetric π-ligand but also for isospecific catalytic systems based on C_1-symmetric π-ligands, like Me_2Si(3-*tert*-butylcyclopentadienyl)(fluorenyl).[8o]

The higher regiospecificities of titanocene based, with respect to zirconocene and hafnocene based, catalytic systems have been accounted for by the large contributions of the nonbonded

† Università di Salerno.
‡ Università di Napoli Federico II.
§ G. Natta Research Center.
⊗ Abstract published in *Advance ACS Abstracts,* April 15, 1997.

(1) Presented in part at the Mario Farina Memorial Symposium on Materials Chirality, American Chemical Society National Meeting, Orlando, Aug. 25−30, 1996.

(2) (a) Ewen, J. *J. Am. Chem. Soc*. **1984**, *106*, 6355. (b) Ewen, J. U.S. Patent 4,522,982 to Exxon, 1985. (c) Ewen, J. In *Catalytic Polymerization of Olefins, Studies in Surface Science and Catalysis*; Keii, T., Soga, K., Eds.; Elsevier: New York, 1986; Vol. 25, p 271. (d) Ewen, J.; Haspeslagh, L.; Atwood, J.; Zhang, H. *J. Am. Chem. Soc*. **1987**, *109*, 6544. (e) Ewen, J.; Haspeslagh, L.; Elder, M.; Atwood, J.; Zhang, H.; Cheng, H. In *Transition Metals and Organometallics as Catalysts for Olefin Polymerization*; Kaminsky, W., Sinn, H., Eds.; Springer-Verlag: Berlin 1988; p 281. (f) Ewen, J.A. *Makromol. Chem. Macromol. Symp.* **1995**, *89*, 181.

(3) (a) Kaminsky, W.; Külper, K.; Brintzinger, H. H.; Wild, F. *Angew. Chem., Int. Ed. Engl.* **1985**, *24*, 507. (b) Kaminsky, W.; Külper, K.; Buschermöhle, M.; Lüker, H. U.S. Patent 4,769,510 to Hoechst, 1988. (c) Kaminsky, W. *Angew. Makromol. Chem.* **1986**, *145/146*, 149. (d) Kaminsky, W. In *Catalytic Polymerization of Olefins*; Keii, Soga, Eds.; Elsevier: New York 1986; p 293.

(4) (a) Schnutenhaus H.; Brintzinger, H. H. *Angew. Chem., Int. Ed. Engl.* **1979**, *18*, 777. (b) Wild, F.; Zsolnai, L.; Huttner, G.; Brintzinger, H. H. *J. Organomet. Chem.* **1982**, *232*, 233. (c) Collins, S.; Kuntz, B.; Taylor, N.; Ward, D. *J. Organomet. Chem.* **1988**, *342*, 21. (d) Wild, F.; Wasiucionek, M.; Huttner, G.; Brintzinger, H. H. *J. Organomet. Chem.* **1985**, *288*, 63. (e) Schäfer, A.; Karl, E.; Zsolnai, L.; Huttner, G.; Brintzinger, H. H. *J. Organomet. Chem.* **1987**, *328*, 87. (f) Wiesenfeldt, H.; Reinmuth, A.; Barsties, E.; Evertz, K.; Brintzinger, H. H. *J. Organomet. Chem.* **1989**, *369*, 359. (g) Burger, P.; Hortmann, K.; Diebold, J.; Brintzinger, H. H. *J. Organomet. Chem.* **1991**, *417*, 9. (h) Brintzinger, H. H. In *Transition Metals and Organometallics as Catalysts for Olefin Polymerization*; Kaminsky, W., Sinn, H., Eds.; Springer-Verlag: Berlin 1988; p 249.

(5) (a) Corradini, P.; Guerra, G.; Vacatello, M.; Villani, V. *Gazz. Chim. Ital.* **1988**, *118*, 173. (b) Cavallo, L.; Guerra, G.; Oliva, L.; Vacatello, M.; Corradini, P. *Polym. Commun.* **1989**, *30*, 16. (c) Cavallo, L.; Corradini, P.; Guerra, G.; Vacatello, M. *Polymer* **1991**, *32*, 1329. (d) Cavallo, L.; Guerra, G.; Vacatello, M.; Corradini, P. *Chirality* **1991**, *3*, 299. (e) Guerra, G.; Cavallo, L.; Moscardi, G.; Vacatello, M.; Corradini, P. *J. Am. Chem. Soc.* **1994**, *116*, 2988. (f) Cavallo, L.; Guerra, G. *Macromolecules* **1996**, *29*, 2729. (g) Cavallo, L.; Corradini, P.; Guerra, G.; Resconi, L. *Organometallics* **1996**, *15*, 2254. (h) Guerra, G.; Cavallo, L.; Moscardi, G.; Vacatello, M.; Corradini, P. *Macromolecules* **1996**, *29*, 4834. (i) Cavallo, L.; Guerra; Corradini, P. *Gazz. Chim. Ital.* **1996**, *126*, 463.

(6) (a) Castonguay, L.; Rappé, A. *J. Am. Chem. Soc.* **1992**, *114*, 5832. (b) Hart, J.; Rappé, A. *J. Am. Chem. Soc.* **1993**, *115*, 6159. (c) Kawamura-Kuribayashi, H.; Koga, N.; Morokuma, K. *J. Am. Chem. Soc.* **1992**, *114*, 8687.

(7) (a) Zambelli, A.; Ammendola, P.; Grassi, A.; Longo, P.; Proto, A. *Macromolecules* **1986**, *19*, 2703. (b) Longo, P.; Grassi, A.; Pellecchia, C.; Zambelli, A. *Macromolecules* **1987**, *20*, 1015.

S0002-7863(96)04142-X CCC: $14.00

interactions, in favor of the monomer coordination suitable for the primary insertion, when shorter Mt−C distances (of nearly 0.1 Å) are involved.[5e]

For the two isospecific catalytic systems based on *rac*-ethylenebis(1-indenyl)$ZrCl_2$[8b,l] or *rac*-ethylenebis(4,5,6,7-tetrahydro-1-indenyl)$ZrCl_2$[8a,b] and MAO, a complete determination of the stereochemical configuration of the regioirregular units has been reported. The three types of microstructures corresponding to the regioirregularities in iPP are shown in Figure 1. These analyses show, among other things, that, for these isospecific catalysts, primary and secondary insertions of propene occur with opposite enantiofaces.

Also this aspect of the isospecific homogeneous polymerization has been rationalized by some by a molecular mechanics analysis, in terms of different enantioselectivity mechanisms for the primary and secondary insertions. In particular, the considered model catalytic complexes indicate a direct interaction of the π-ligands with the methyl group of the monomer for the secondary insertion while this interaction is mediated by the *chiral orientation of the growing chain* for the primary insertion.[5e]

The dependence of the regiospecificity (as well as of the stereospecificity) on the monomer concentration and on the temperature in propene polymerization has been reported by one of us for the *rac*-ethylenebis(1-indenyl)$ZrCl_2$/MAO catalyst.[9,10] It has been found that the total amount of regioirregularities does not depend on monomer concentration, while a dependence on polymerization temperature has been found. On the other side, the relative amounts of 2,1 and 3,1 regiodefects depend on both polymerization temperature and monomer concentration.

The high regiospecificity of Ewen's syndiospecific catalysts has been reported several times in the literature.[11] Also for several aspecific catalytic systems, as for instance those based on two unbridged Cp or Cp^* ligands[3,12] or on *meso*-ethylenebis-(4,4,6,7-tetrahydro-1-indenyl),[13] the regiospecificity is generally higher than for the isospecific catalysts.

The regioirregularities can be reduced, but generally not suppressed to levels below the detection limit, also for isospecific catalysts based on *ansa*-zirconocenes when the C_2 symmetric ligand contains at each ring ligand, in addition to substituents in the 4 (β) positions (which is determining for the enantioselectivity), a methyl group in the 2 (α) position.[14]

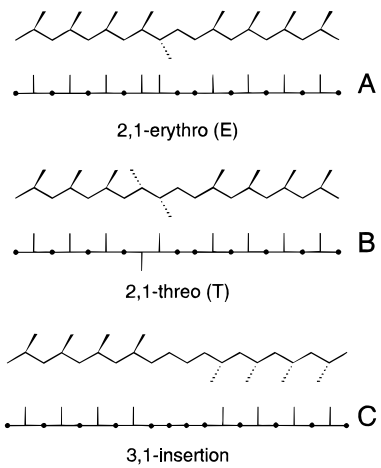

Figure 1. Trans-planar (top) and modified Fisher (bottom) representations of chain segments generated by isolated secondary (2,1) insertion: (A) erythro (meso); (B) threo (racemic); and (C) 3,1 unit. The polymer chain start is on the right of the chain segment, and the chain end generated by chain transfer is on the left.

In the first part of this paper the amount and type of regioirregularities of polypropene samples from polymerizations in similar conditions with several zirconocene-based catalytic systems (aspecific syndiospecific and isospecific) are compared. The aim is to verify the possible dependence of the amount of regioirregularities on the type of stereospecificity.

In the second part of this paper, a molecular mechanics analysis on model catalytic complexes corresponding to aspecific, syndiospecific, and isospecific catalytic systems, respectively, is presented. In particular, the analysis aims to compare possible alkene-bound intermediates as well as situations closer to the transition states of the primary and secondary monomer insertions (pre-insertion intermediates).

In the third part of this paper a possible rationalization of the observed dependence of the degree of regiospecificity on the type of stereospecificity is presented. This is based on the results of the molecular mechanics analyses and requires the assumption that the activation energy for the rotation of the coordinated monomer between the orientation suitable for the primary and secondary insertion is in general lower than (or comparable to) the activation energy for the secondary monomer insertion.

Results

Regiospecificity of Catalytic Systems Based on Zirconocenes and Hafnocenes. Our investigation of metallocene-catalyzed propene polymerization was conducted with the polymerization procedure (liquid monomer, prereacted catalyst/cocatalyst, 50 °C, 1 h) described in detail in ref 9. Details of the polymer analysis are also described in ref 9.

All the considered achiral, C_{2v} symmetric zirconocenes and hafnocenes, whether bridged or unbridged, substituted and unsubstituted, always produce atactic polypropenes with no detectable secondary units, not even as chain end groups. In particular, this has been observed for the catalysts Cp_2ZrCl_2, Cp_2HfCl_2, Cp_2*ZrCl_2, Cp_2*HfCl_2, $Me_2Si(Cp)_2ZrCl_2$, $Me_2Si(Cp*)_2ZrCl_2$, $Me_2C(Cp)_2ZrCl_2$, $Me_2Si(Flu)_2ZrCl_2$, and $En(Flu)_2ZrCl_2$, where Me, Cp, Cp*, and Flu indicate methyl group,

(8) (a) Soga, K.; Shiono, T.; Takemura, S.; Kaminsky, W. *Makromol. Chem., Rapid Commun.* **1987**, *8*, 305. (b) Grassi, A.; Zambelli, A.; Resconi, L.; Albizzati, E.; Mazzocchi, R. *Macromolecules* **1988**, *21*, 617. (c) Cheng, H.; Ewen, J. *Makromol. Chem.* **1989**, *190*, 1931. (d) Tsutsui, T.; Ishimaru, N.; Mizuno, A.; Toyota, A.; Kashiwa, N. *Polymer* **1989**, *30*, 1350. (e) Tsutsui, T.; Mizuno, A.; Kashiwa, N. *Makromol. Chem.* **1989**, *190*, 1177. (f) Tsutsui, T.; Kioka, M.; Toyota, A.; Kashiwa, N. In *Catalytic Olefin Polymerization, Studies in Surface Science and Catalysis;* Keii, T., Soga, K., Eds.; Elsevier: New York, 1990; Vol. 56, p 493. (g) Rieger, B.; Chien, J. *Polym. Bull.* **1989**, *21*, 159. (h) Rieger, B.; Mu, X.; Mallin, D.; Rausch, M.; Chien, J. *Macromolecules* **1990**, *23*, 3559. (i) Chien, J.; Sugimoto, R. *J. Polym. Sci. A*: *Polym. Chem.* **1991**, *29*, 459. (j) Mizuno, A.; Tsutsui, T.; Kashiwa, N. *Polymer* **1992**, *33*, 254. (k) Busico, V.; Cipullo, R. *J. Organomet. Chem.* **1995**, *497*, 113. (l) Up to 20% 1,3 units have been observed with a highly hindered system: Spaleck, W.; Antberg, M.; Aulbach, M.; Bachmann, B.; Dolle, V.; Haftka, S.; Küber, F.; Rohrmann, J.; Winter, A. In *Ziegler Catalysts*; Fink, Mülhaupt, Brintzinger, Eds.; Springer-Verlag: Berlin, 1995; p 83. (m) Razavi, A.; Vereecke, D.; Peters, L.; Den Davw, K.; Nafpliotis, L.; Atwood, J. L. In *Ziegler Catalysts*; Fink, Mülhaupt, Brintzinger, Eds.; Springer-Verlag: Berlin, 1995; p 111.

(9) Resconi, L.; Fait, A.; Piemontesi, F.; Colonnesi, M.; Rychlicki, H.; Zeigler, R. *Macromolecules* **1995**, *28*, 6667.

(10) (a) Resconi, L.; Piemontesi, F.; Camurati, I.; Rychlicki, H.; Colonnesi, M.; Balboni, D. *Polym. Mater. Sci. Eng.* **1995**, *73*, 516. (b) Resconi, L.; Piemontesi, F.; Camurati, I.; Balboni, D.; Sironi, A.; Moret, M.; Rychlicki, H.; Zeigler, R. *Organometallics* **1996**, *15*, 5046.

(11) (a) Ewen, J. A.; Elder, M. J.; Jones, R. L.; Curtis, S.; Cheng, H. N. In *Catalytic Olefin Polymerization, Studies in Surface Science and Catalysis;* Keii, T., Soga, K., Eds.; Elsevier: New York, 1990; Vol. 56, p 439. (b) Herfert, N.; Fink, G. *Makromol. Chem.* **1992**, *193*, 773.

(12) Resconi, L.; Piemontesi, F.; Franciscono, G.; Abis, L.; Fiorani, T. *J. Am. Chem. Soc.* **1992**, *114*, 1025.

(13) Lee, I. M.; Gauthier, W. J.; Ball, J. M.; Iyengar, B.; Collins, S. *Organometallics* **1992**, *11*, 2115.

(14) (a) Röll, W.; Brintzinger, H. H.; Rieger B.; Zolk, R. *Angew. Chem., Int. Ed. Engl.* **1990**, *29*, 279. (b) Stehling, V.; Diebold, J.; Kirsten, R.; Röll, W.; Brintzinger, H. H. *Organometallics* **1994**, *13*, 964.

Table 1. Propylene Polymerization with Racemic Zirconocene/MAO Catalysts[a]

zirconocene	tacticity[b] mmmm	total regioirr units,[c]%	ref
$Me_2C(Ind)_2ZrCl_2$	80.6_9	0.4	10b
$C_2H_4(Ind)_2ZrCl_2$[d]	87.5_5	0.5_5	9, 10a
$C_2H_4(H_4Ind)_2ZrCl_2$	91.5_0	0.9_7	10b
$C_2H_4(4,7\text{-}Me_2\text{-}Ind)_2ZrCl_2$[d]	91.8_4	2.8_0[e]	10c
$Me_2Si(Ind)_2ZrCl_2$	90.3_0	0.4_8	10c
$Me_2Si(H_4Ind)_2ZrCl_2$	94.9_1	0.5_4	10c
$Me_2Si(4,7\text{-}Me_2Ind)_2ZrCl_2$	91.3_9	1.8_4[e]	10c
$Me_2Si(2\text{-}Me\text{-}Ind)_2ZrCl_2$	94.2_5	0.3_3	10b
$C_2H_4(3\text{-}Me\text{-}Ind)_2ZrCl_2$	19.9_6	0	10a

[a] Polymerization conditions: 1-L stainless-steel autoclave, propene 0.4 L, 50 °C, 1 h, zirconocene/MAO aged 10 min. [b] Determined assuming the enantiomorphic site model, see ref 9. [c] Determined as described in ref 9. [d] Average values. [e] End groups included.

cyclopentadienyl, pentamethylcyclopentadienyl, and fluorenyl ligands, respectively.

The high regiospecificity of Ewen's syndiospecific C_s symmetric catalyst ($Me_2C(CpFlu)ZrCl_2$) has been confirmed for polymerization temperatures in the range 0−70 °C. In fact in all the obtained polymer samples, also in the ethyl acetate soluble fraction of the polymer obtained at 70 °C (20% b.w.), regioirregularities were not detected.

The relevant microstructural features of polymer samples obtained with racemic isospecific C_2 symmetric *ansa*-zirconocenes, under our standard polymerization conditions, are reported in Table 1. The isospecificity of the catalysts is defined by the statistical parameter *b*, which represents the probability of a correct monomer insertion and has been evaluated by the experimental pentad distribution in the frame of enantiomorphic-site control.[9,10]

It is noteworthy that all the isospecific catalysts present easily detectable amounts of regioirregularities with the exception of ethylenebis(3-methylindenyl)$ZrCl_2$, which is, however, poorly isospecific.

Molecular Mechanics Analysis. (a) Models. As in previous papers,[5] the basic models of the alkene-bound intermediates considered in this paper are metal complexes containing three ligands, that is a π-coordinated propene molecule, a σ-coordinated isobutyl group (simulating a primary growing chain), and a stereorigid π-coordinated ligand. In order to simplify the following discussion, the considered aspecific, syndiospecific, and isospecific model complexes present C_{2v}, C_s, or C_2 symmetry, respectively. Moreover, for the sake of an easier comparison, all the considered catalytic complexes present a bridged π-ligand and the bridge is identical in all cases (just as an example the dimethylsilyl bridge has been considered). However, the conclusions relative to the present calculations are substantially independent of the type of symmetry, as well as of the kind of bridge, and can also be extended to the usual aspecific catalytic complexes with unbridged π-ligands.

We recall the definitions of the most important internal coordinates that have been varied (see Figure 2): the dihedral angle θ_0 associated with rotations of the olefin around the axis connecting the metal to the center of the double bond, and the internal rotation angle θ_1 associated with rotations around the bond between the metal atom and the first carbon atom of the growing chain. At θ_0 near 0° the olefin is oriented in a position suitable for primary insertion, while θ_0 near 180° corresponds to an orientation suitable for secondary insertion. θ_1 near 0° corresponds to the conformation having the first C−C bond of the growing chain eclipsed with respect to the axis connecting the metal atom to the center of the double bond of the olefin.

A prochiral olefin such as propene may give rise to non-superposable coordinations, which can be labeled with the notation *re* and *si*.[15] The coordination of the C_2 symmetric ligand is chiral and can be labeled with the notation (*R)* or (*S)* according to the rules of Cahn−Ingold−Prelog[16] extended to chiral metallocenes as outlined by Schlögl.[17] The symbols (*R*) and (*S*) indicate the absolute configuration of the bridgehead carbon atom of the indenyl groups, for the C_2 symmetric ligand. Without loss of generality, all the reported calculations refer to the (*R,R*) coordination of the C_2 symmetric ligand. Finally, in the case of the C_s symmetric ligand, an intrinsic chirality at the central metal atom is present, which can be labeled with the notation *R* or *S*, by an extension of the Cahn−Ingold−Prelog rules, as proposed by Stanley and Baird.[18] This nomenclature has been used by us to distinguish the enantiomeric alkene-bound intermediates that may arise by exchanging the relative positions of the growing chain and of the incoming monomer.[19] However, without loss of generality, all the reported calculations refer to the *R* chirality at the metal atom.

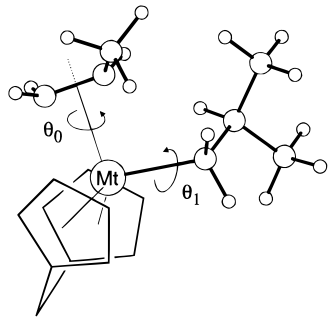

Figure 2. One of the model catalytic complexes used in our computations comprised of the $Me_2Si(Cp)_2$ ligand, a propene molecule (shown for the *re*-coordination), and an alkyl group simulating the growing chain. The dihedral angle θ_0 associated with rotations of the olefin around the axis connecting the metal to the center of the double bond and the internal rotation angle θ_1 associated with rotations around the bond between the metal atom and the first carbon atom of the growing chain are indicated. The conformation depicted corresponds to $\theta_0 = 0°$ and $\theta_1 = -60°$ (suitable for the monomer primary insertion).

We also recall that, in the framework of our analysis, the conformations of alkene-bound intermediates are considered sufficiently close to the transition state, and considered as suitable conformers of **pre-insertion intermediates**, only if the insertion can occur through a process of "least nuclear motion".[20] This corresponds to geometries of the alkene-bound intermediates for which[20a,d,e] (i) the double bond of the olefin is nearly parallel to the bond between the metal atom and the growing chain ($\theta_0 \approx 0°$ or $\theta_0 \approx 180°$) and (ii) the first C−C bond of the chain is nearly perpendicular to the plane defined by the double bond of the monomer and by the metal atom ($|\theta_1| \approx 60-90°$ rather than $\theta_1 \approx 180°$). Let us recall that θ_1 values away from 180° and near 60° are also suited for the formation of an α-agostic bond, which has been shown to stabilize the transition state for the insertion step in some scandium- and zirconium-based catalysts.[21]

Moreover, alkene-bound intermediates for which the methyl group of the propene and the second carbon atom (and its

(15) Hanson, K. R. *J. Am. Chem. Soc.* **1966**, *88*, 2731.
(16) (a) Cahn, R. S.; Ingold, C.; Prelog, V. *Angew. Chem., Int. Ed. Engl.* **1966**, *5*, 385. (b) Prelog, V.; Helmchem, G. *Angew. Chem., Int. Ed. Engl.* **1982**, *21*, 567.
(17) Schlögl, K. *Top. Stereochem.* **1966**, *1*, 39.
(18) Stanley, K.; Baird, M. C. *J. Am. Chem. Soc.* **1975**, *97*, 6598.
(19) Cavallo, L.; Corradini, P.; Guerra, G.; Vacatello, M. *Macromolecules* **1991**, *24*, 1784.
(20) (a) Cossee, P. *Tetrahedron Lett.* **1960**, *17*, 12. (b) Cossee, P. *Tetrahedron Lett.* **1960**, *17*, 17. (c) Cossee, P. *J. Catal.* **1964**, *3*, 80. (d) Hine, J. *J. Org. Chem.* **1966**, *31*, 1236. (e) Hine, J. *Adv. Phys. Org. Chem.* **1977**, *15*, 1. (f) Venditto, V.; Guerra, G.; Corradini, P.; Fusco, R. *Polymer* **1990**, *31*, 530. (g) Venditto, V.; Guerra, G.; Corradini, P.; Fusco, R. *Eur. Polym. J.* **1991**, *27*, 45.

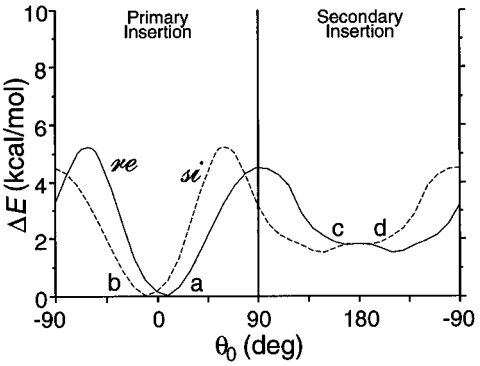

Figure 3. The optimized energies plotted as a function of θ_0 for the model complex with the $Me_2Si(Cp)_2$ ligand (aspecific). The full and dashed lines refer to *re*- and *si*-coordinated propene, respectively. The models corresponding to situations with $\theta_0 \approx 0°$, labeled a and b, are sketched in Figure 4, parts A and B, respectively. The models corresponding to situations with $\theta_0 \approx 180°$, labeled c and d, are sketched in Figure 4, parts C and D, respectively.

substituents) of the growing chain are on the same side with respect to the plane defined by the Mt−C bonds ($\theta_1 \approx +60°$ and $-60°$ for the *re* and *si* coordinated monomer, respectively) are assumed to be unsuitable for successive monomer insertion. In fact, the insertion paths starting from these intermediates involve large nonbonded interactions.[22,20f,g]

We assume that the energy differences between suitable pre-insertion intermediates are close to those present in the corresponding transition states for the insertion reaction.

All the reported energy curves are versus the dihedral angle θ_0 associated with rotations of the olefin around the axis connecting the metal to the center of the double bond.

(b) Aspecific Catalytic Complex. Figure 3 plots as a function of θ_0 the fully optimized energies for the model complex with the $Me_2Si(Cp)_2$ ligand, that is a π-ligand with C_{2v} symmetry. Of course, energetically equivalent situations are obtained for *re* and *si* propene coordinations, since this chirality is the only one present in the model.

The enantiomeric coordination intermediates, labeled a and b in Figure 3, with $\theta_0 \approx 0°$ (propene orientation suitable for its primary insertion) are of lower energy than the enantiomeric minimum energy situations, labeled c and d in Figure 3, with $\theta_0 \approx 180°$ (propene orientation suitable for its secondary insertion).

Models corresponding to the situations labeled a, b, c, and d in Figure 3 are sketched in Figure 4, parts A, B, C, and D, respectively. The models in Figure 4, parts A and B, minimize the interactions between the growing chain (at $\theta_1 \approx -60°$ and at $\theta_1 \approx +60°$) and the methyl of the propene monomer (*re* and *si* coordinated, respectively). Therefore, as previously discussed, they are both assumed to be pre-insertion intermediates suitable for the primary insertion reaction. The models in Figure 4, parts C and D, independently of the orientation of the growing chain (with $\theta_1 \approx -60°$ or with $\theta_1 \approx +60°$) are assumed to be pre-insertion intermediates suitable for the secondary insertion reaction.

Hence, for this aspecific model the pre-insertion intermediates suitable for (and perhaps relevant to) the primary monomer insertion are favored with respect to the pre-insertion intermediates suitable for the secondary monomer insertion (of nearly 2 kcal/mol). This energy difference, in the framework of the assumed mechanism, can give a rough estimate of the non-bonded energy contribution to the regiospecificity of the insertion reaction.

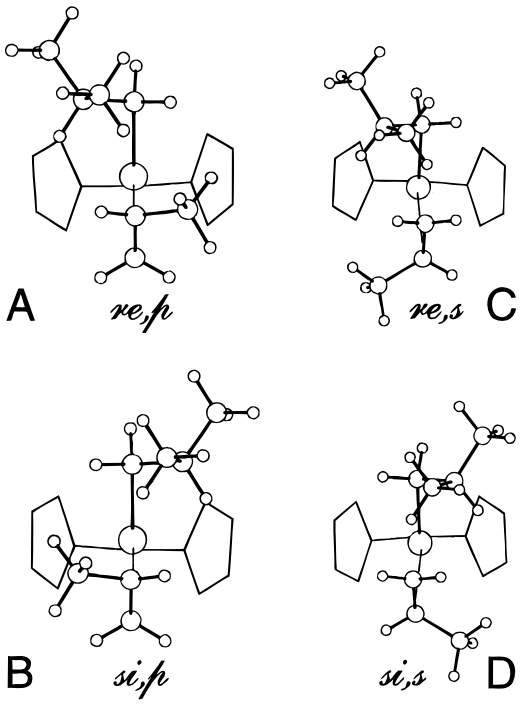

Figure 4. Alkene-bound intermediates for both propene enantiofaces (*re* and *si*) with monomer orientations suitable for primary (*p*) and secondary (*s*) insertions into a primary polypropene growing chain for the case of the aspecific ligand. Models A−D correspond to the situations labeled a−d in Figure 3. All models are suitable for monomer insertion (pre-insertion intermediates, see text).

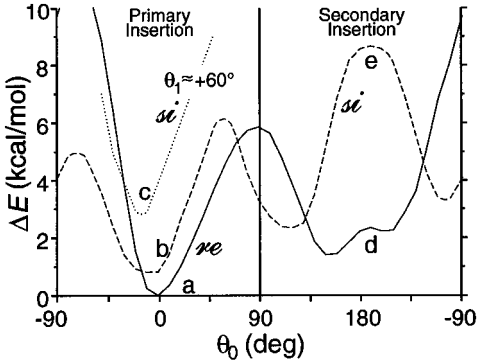

Figure 5. The optimized energies as a function of θ_0 for the model complex with the $Me_2Si(Cp)(Flu)$ ligand (syndiospecific) for the *R* chirality at the metal atom. The full and dashed lines refer to *re*- and *si*-coordinated propene, respectively. The dotted line is a part of the optimized energy curve obtained by requiring, for the *si*-coordinated monomer, that the methyl group of the propene and the second carbon atom (and its substituents) of the growing chain are on opposite sides with respect to the plane defined by the Zr−C bonds (i.e., requiring $\theta_1 \approx +60°$). The models corresponding to situations with $\theta_0 \approx 0°$, labeled a, b, and c, are sketched in Figure 6, parts A, B, and C, respectively. The models corresponding to situations with $\theta_0 \approx 180°$, labeled d and e, are sketched in Figure 6, parts D and E, respectively.

(c) Syndiospecific Catalytic Complex. Figure 5 plots as a function of θ_0 the fully optimized energies for the model complex with the $Me_2Si(Cp)(Flu)$ ligand, that is a π-ligand with C_s symmetry, for the polymerization step involving an *R* chirality at the metal atom.

The absolute minimum energy, labeled a, corresponds to $\theta_0 \approx 0°$, for the *re*-monomer coordination, and the corresponding

(21) (a) Kraudelat, H.; Brintzinger, H. H. *Angew. Chem., Int. Ed. Engl.* **1990**, *29*, 1412. (b) Brintzinger, H. H.; Fischer, D.; Mülhaupt, R.; Rieger, B.; Waymouth, R. M. *Angew. Chem., Int. Ed. Engl.* **1995**, *34*, 1143 (c) Piers, W. E.; Bercaw, J. E. *J. Am. Chem. Soc.* **1990**, *112*, 9406. (d) Clawson, L.; Soto, J.; Buchwald, S. L.; Steigerwald, M. L.; Grubbs, R. H. *J. Am. Chem. Soc.* **1985**, *107*, 3377.

(22) (a) Corradini, P.; Barone, V.; Fusco, R.; Guerra, G. *Eur. Polym. J.* **1979**, *15*, 133. (b) Corradini, P.; Barone, V.; Fusco, R.; Guerra, G. *Gazz. Chim. Ital.* **1983**, *113*, 601.

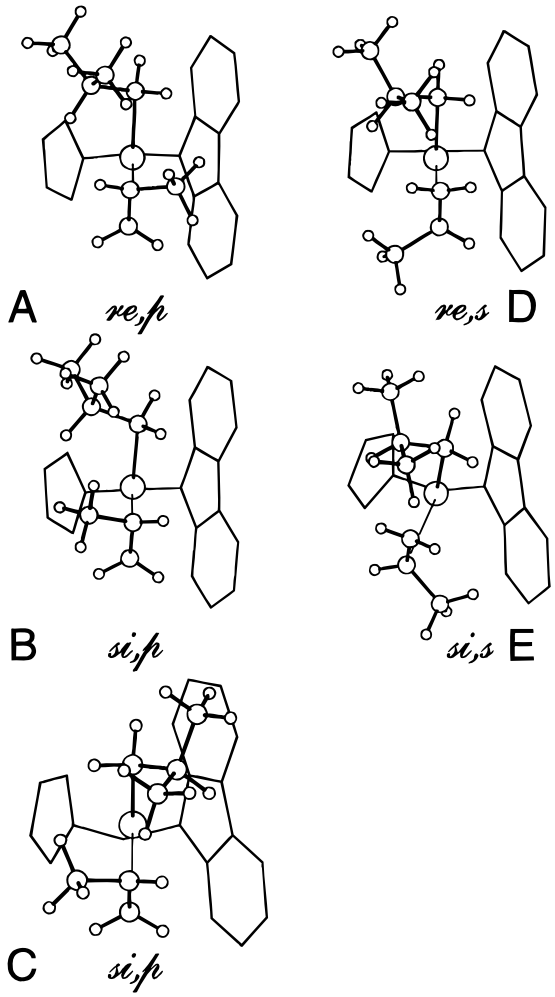

Figure 6. Alkene-bound intermediates for both propene enantiofaces (*re* and *si*) with monomer orientations suitable for primary (*p*) and secondary (*s*) insertions into a primary polypropene growing chain, for the case of the syndiospecific ligand for *R* chirality at the metal atom. Models A−E correspond to the situations labeled a−e in Figure 5. Models A and D (both with *re*-coordinated propene) correspond to the minimum energy pre-insertion intermediates for primary and secondary monomer insertion, respectively.

model is sketched in Figure 6A. This model minimizes the interactions between the growing chain (at $\theta_1 \approx -60°$) and the methyl of the propene monomer (*re* coordinated). Therefore, it is assumed to be a pre-insertion intermediate suitable for the *re*-monomer primary insertion.

A slightly higher energy is calculated for the minimum energy, labeled b in Figure 5, which corresponds to $\theta_0 \approx 0°$ and $\theta_1 \approx -60°$, for the *si*-monomer coordination. The corresponding model of coordination intermediate, sketched in Figure 6B, is, however, considered unsuitable for the successive monomer insertion reaction. In fact, the methyl group of the propene and the second carbon atom (and its substituents) of the growing chain are on the same side with respect to the plane defined by the Zr−C bonds.

The optimized energy curve obtained by requiring, for the *si*-coordinated monomer, that the methyl group of the propene and the second carbon atom (and its substituents) of the growing chain are on opposite sides with respect to the plane defined by the Zr−C bonds (i.e., requiring $\theta_1 \approx +60°$) is also shown in Figure 5 as a dotted line. The energy minimum, labeled c, is nearly 3 kcal/mol higher than the absolute minimum and the corresponding model is sketched in Figure 6C. This model minimizes the interactions between the growing chain (at $\theta_1 \approx +60°$) and the methyl of the propene monomer (*si* coordinated). Therefore, it is assumed to be a pre-insertion intermediate suitable for the *si*-monomer primary insertion.

Due to the presence of a local C_s symmetry plane, the two coordination positions available for the coordination of the monomer and of the growing chain are enantiotopic. In the framework of the polymerization mechanism involving a *chain migratory insertion*, most consecutive polymerization steps correspond to models obtained by exchanging the relative positions of the growing chain and of the incoming monomer, that is to models with opposite chirality at the metal atom. Hence, as already discussed in ref 19, the calculated enantioselectivity of a given insertion step assures the syndiospecificity of the model.

The optimized energy corresponding to $\theta_0 = 180°$ for the *re*-monomer coordination, labeled d in Figure 5, is higher by nearly 2 kcal/mol with respect to the absolute minimum. The corresponding model sketched in Figure 6D is considered as suitable for the *re*-monomer secondary insertion.

As already shown by less accurate calculations on a simpler syndiospecific model including a methyl group (simulating the growing chain) and the isopropyl(Cp)(Flu) ligand,[19] the *si*-monomer coordination situation with θ_0 close to 180° (labeled e in Figure 5) is of high energy. The corresponding model shown in Figure 6E clearly shows that the high energies are due to the repulsive interactions of the methyl group of propene with one of the six-membered rings of the fluorenyl ligand. The distortion of the coordination of the bridged π-ligand, due to the large nonbonded interactions, is very apparent from the sketch.

In summary, there is a substantial enantioselectivity of this syndiospecific catalytic model for the lower energy (and experimentally observed) primary monomer insertion and the enantioselectivity would also be higher for the higher energy (experimentally undetected) secondary monomer insertion.

It is relevant to note that the enantioselectivity of the syndiospecific model site is in favor of the same monomer prochiral face, for both primary and secondary insertions. The interactions of the methyl substituent of the coordinated propene that generate the enantioselectivity are different, however: with the chirally oriented growing chain, for the primary insertion, and with one of the six-membered rings of the π-ligand, for the secondary insertion.

As for the aspecific model of the previous section, also for this syndiospecific model there is an energy difference (≈2 kcal/mol) in favor of the pre-insertion intermediate for the primary insertion, which gives a possible estimate of the nonbonded energy contribution to regiospecificity.

(d) Isospecific Catalytic Complex. Figure 7 plots as a function of θ_0 the fully optimized energies for the model complex with the $Me_2Si(Ind)_2$ ligand, that is a π-ligand with C_2 symmetry, with (*R*,*R*) chirality of coordination of the π ligand.

As for the syndiospecific model of Figure 5, the absolute minimum energy, labeled a in Figure 7, corresponds to $\theta_0 \approx 0°$, for the *re*-monomer coordination; the corresponding model is sketched in Figure 8A. This model minimizes the interactions between the growing chain (at $\theta_1 \approx -60°$) and the methyl of the propene monomer (*re* coordinated). Therefore, it is assumed to be a pre-insertion intermediate suitable for the *re*-monomer primary insertion.

Again as for the syndiospecific model of Figure 5, a slightly higher energy is calculated for the minimum energy, labeled b in Figure 7, which corresponds to $\theta_0 \approx 0°$ and $\theta_1 \approx -60°$, for the *si* monomer coordination (sketched in Figure 8B), which is, however, considered unsuitable for the successive monomer insertion. The optimized energy curve obtained by requiring,

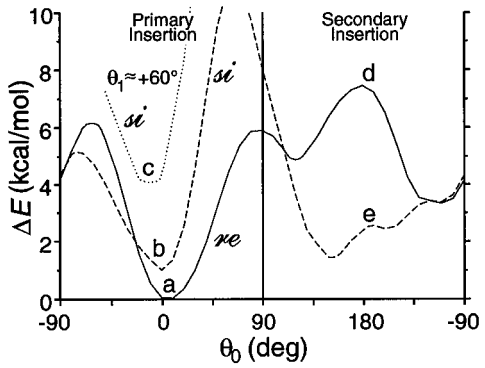

Figure 7. The optimized energies plotted as a function of θ_0 for the model complex with the (*R*,*R*) coordinated $Me_2Si(Ind)_2$ ligand (isospecific). The full and dashed lines refer to *re*- and *si*-coordinated propene, respectively. The dotted line is a part of the optimized energy curve obtained by requiring, for the *si* coordinated monomer, that the methyl group of the propene and the second carbon atom (and its substituents) of the growing chain are on opposite sides with respect to the plane defined by the Zr−C bonds (i.e., requiring $\theta_1 \approx +60°$). The models corresponding to situations with $\theta_0 \approx 0°$, labeled a, b, and c, are sketched in Figure 8, parts A, B, and C, respectively. The models corresponding to situations with $\theta_0 \approx 180°$, labeled d and e, are sketched in Figure 8, parts D and E, respectively.

for the *si* coordinated monomer, $\theta_1 \approx +60°$ is also shown in Figure 7 as a dotted line. The energy minimum, labeled c, is nearly 4 kcal/mol higher than the absolute minimum, and the corresponding model, sketched in Figure 8C, is assumed to be a pre-insertion intermediate suitable for the *si*-monomer primary insertion.

As already discussed in ref 5, due to the presence of a local C_2 symmetry axis the two coordination positions available for the coordination of the monomer and of the growing chain are homotopic. That is, models obtained by exchanging the relative positions of the growing chain and of the incoming monomer (which in the framework of the polymerization mechanism involving a *chain migratory insertion* correspond to consecutive polymerization steps) are identical. Hence the calculated enantioselectivity of a given insertion step assures the isospecificity of the model.

The optimized energy corresponding to $\theta_0 = 180°$ for the *si*-monomer coordination, labeled e in Figure 7, is higher by nearly 2 kcal/mol with respect to the absolute minimum. The corresponding model sketched in Figure 8E is considered as suitable for *si*-monomer secondary monomer insertion.

As already discussed in detail for the isospecific model sites, including the ethylenebis(1-indenyl) and ethylenebis(4,5,6,7-tetrahydro-1-indenyl) ligands,[5e] the energy is higher, corresponding to $\theta_0 = 180°$, for the *re* monomer coordination (the situation labeled d in Figure 7). The corresponding model shown in Figure 8D, which presents large distortions in the coordination of the bridged π-ligand, clearly shows that the high energies are mainly due to the repulsive interactions of the methyl group of propene with the six-membered rings of one of the indenyl ligands.

In summary, there is a substantial enantioselectivity of this isospecific catalytic model for the lower energy (and experimentally observed) primary monomer insertion, and the enantioselectivity would also be higher for the higher energy (experimentally detected) secondary monomer insertion.

It is worth noting that the enantioselectivity of the isospecific model site (contrary to the syndiospecific model site) is in favor of opposite monomer prochiral faces, for primary and secondary insertions.

As already discussed in ref 5e, this result is in perfect agreement with the observed microstructure of polypropene

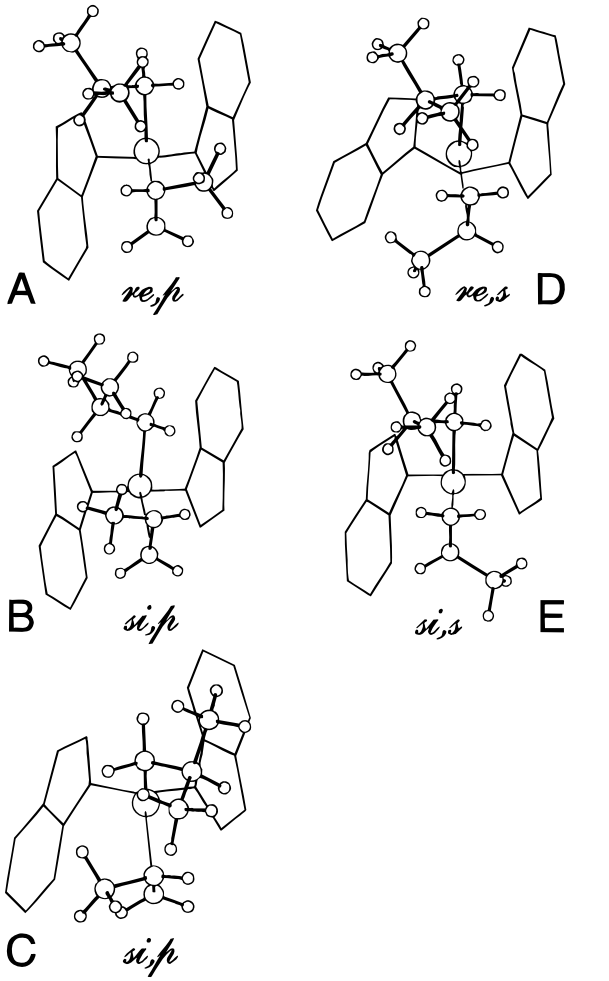

Figure 8. Alkene-bound intermediates for both propene enantiofaces (*re* and *si*) with monomer orientations suitable for primary (*p*) and secondary (*s*) insertions into a primary polypropene growing chain, for the case of the (*R*,*R*) coordinated isospecific ligand. Models A−E correspond to the situations labeled a−e in Figure 7. Models A and E (with opposite propene enantiofaces) correspond to the minimum energy pre-insertion intermediates for primary and secondary monomer insertion, respectively.

chains obtained by isospecific catalytic systems, including the aforementioned analogous bridged π-ligands. Moreover, the nonbonded interactions generating enantioselectivity are those between the methyl substituent of the coordinated propene and (as found for the syndiospecific model of the previous section) the chiral oriented growing chain, in the case of primary insertion, and those between the propene methyl group and one of the six-membered rings of the π-ligand, in the case of secondary insertion.

As for the aspecific and syndiospecific models of the previous sections, for the isospecific model there is an energy difference in favor of the pre-insertion intermediate for the primary insertion, which gives an estimate of the nonbonded energy contribution to the regiospecificity ($\approx$2 kcal/mol).

It is worth noting that for a typical C_1 symmetric highly isospecific catalytic system, based on the Me_2Si(3-*tert*-butylcyclopentadienyl)(fluorenyl) ligand,[2f,8o] our calculations indicate, as for the C_2 symmetric isospecific model complexes, enantioselectivity in favor of opposite monomer prochiral faces, for primary and secondary insertions.

A Possible Rationalization of the Dependence of the Regiospecificity on the Stereospecificity. As described in the Experimental Section, while the syndiospecific and aspecific zirconocene-based catalytic systems are highly regiospecific, isospecific systems always produce measurable amounts of

regioirregular monomeric units.

This dependence of the degree of regiospecificity on the symmetry rather than on the nature of the π-ligand is, of course, not easy to rationalize by invoking differences in the electronic contributions to the regiospecificity.

On the other hand, the molecular mechanics analysis of the previous section indicates that the nonbonded energy contribution to the differences between the minimum energy secondary and primary pre-insertion intermediates, for zirconocene-based catalytic models, is poorly dependent on the symmetry of the π-ligands and hence on their stereospecificity (in Figures 3 and 5 $E_d - E_a \approx 2$ kcal/mol and in Figure 7 $E_e - E_a \approx 2$ kcal/mol).

However, for the enantioselective (syndiospecific and isospecific) model complexes, this energy difference between secondary and primary pre-insertion intermediates, for a given chirality of coordination of the monomer, largely changes with the symmetry of the π-ligands. In particular, for the syndiospecific and isospecific model complexes, the nonbonded energy contribution to the regioselectivity is particularly large for the enantioface, which is wrong with references to Figure 5, $E_e - E_b \approx 8$ kcal/mol, and right with reference to Figure 7, $E_d - E_a \approx 8$ kcal/mol, for the primary insertion, respectively. Particularly relevant is that, the isospecific model, for the enantioface leading to the wrong primary insertion, the calculated nonbonded energy difference between secondary and primary pre-insertion intermediates becomes negative (with references to Figure 7, $E_e - E_c \approx -1.5$ kcal/mol).

Schematic plots of the internal energy versus the reaction coordinate, for both primary and secondary insertions, for generic aspecific, syndiospecific, and isospecific model complexes are sketched in Figure 9, parts A, B, and C, respectively. The minima at the centers and at the ends of the energy curves correspond to alkene-free intermediates, including a growing chain with n and $n + 1$ monomeric units, respectively. Movements from the central minima toward the left and the right correspond to possible reaction pathways leading to primary and secondary insertions, respectively. For the enantioselective complexes the reaction pathways for monomer enantiofaces being right and wrong for primary insertion are different, and are indicated by full and dashed lines, respectively. The two energy barriers encountered for each pathway correspond to the coordination and insertion steps.

The energy minima between the energy barriers for the monomer coordination and insertion correspond to alkene-bound intermediates of the kind simulated by our molecular mechanics calculations (Figures 3−8). The possible dissociation of the monomer coordinated with the wrong enantioface can lead back to the alkene-free intermediate or, directly, to the alkene-bound intermediate with the right enantioface (through some isomerization mechanism, for which the monomer does not leave the coordination sphere of the metal).

For an easier comparison, the labels a−e used for coordination and pre-insertion intermediates in Figures 3, 5, and 7 are also reported close to the schematic energy plots of Figure 9, parts A, B, and C, respectively. The pre-insertion intermediates of our molecular mechanics analysis (when different from the coordination intermediates) correspond to situations closer to the transition state for the insertion reactions.

In the sketches of Figure 9, the energy minima corresponding to the pre-insertion intermediates for primary insertion of the right monomer enantioface are close in energy to the starting alkene-free intermediate. However, all the considerations which follow hold also for pre-insertion intermediates lower or higher in energy with respect to the starting alkene-free intermediate.

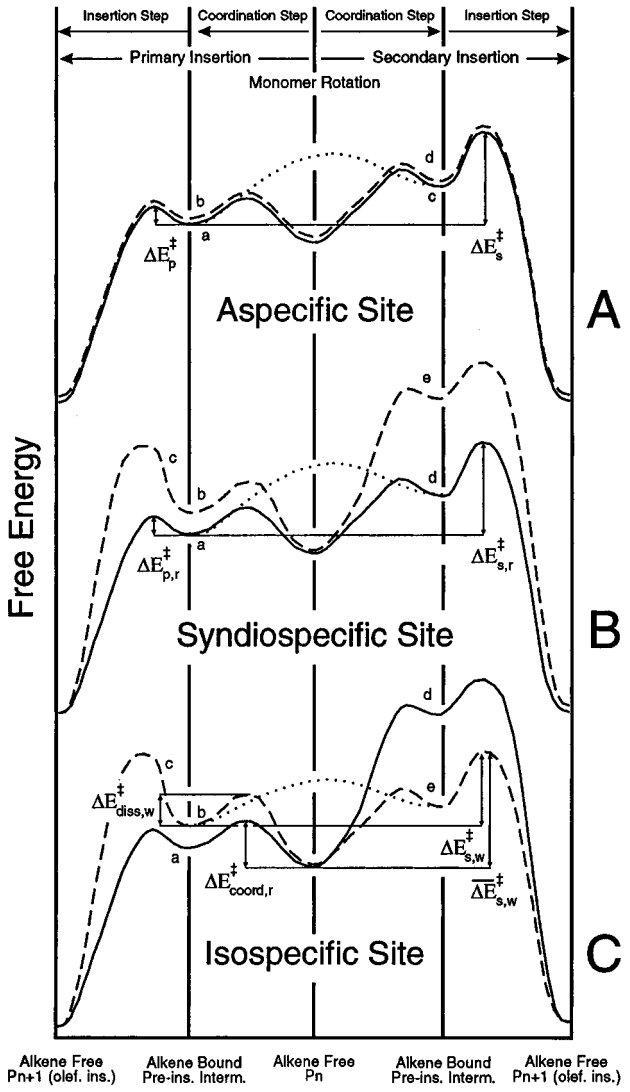

Figure 9. Schematic plots of the internal energy versus the reaction coordinate, for both primary and secondary insertions, for generic aspecific (A), syndiospecific (B), and isospecific (C) model complexes. The minima at the centers and at the ends of the energy curves correspond to alkene-free catalytic intermediates, including a growing chain with n and $n + 1$ monomeric units, respectively. Movements from the central minima toward the left and the right correspond to possible reaction pathways leading to primary and secondary insertions, respectively. For the enantioselective complexes (B, C) the reaction pathways for monomer enantiofaces being right and wrong for primary insertion are different and are indicated by full and dashed lines, respectively. The two energy barriers encountered for each pathway correspond to the coordination and insertion steps. The energy minima between the energy barriers for the monomer coordination and insertion correspond to alkene-bound catalytic intermediates of the kind simulated by our molecular mechanics calculations (Figures 3−8). In particular, the labels a−e close to the curves of parts A, B, and C correspond to the coordination and pre-insertion intermediates of Figures 3, 5, and 7, respectively. The dotted lines indicate the rotation of the coordinated monomer around θ_0 whose activation energy is assumed to be lower than (or comparable to) the activation energy for the secondary insertion. The activation energies, which in this framework are relevant to the regiospecificity, are also indicated.

For the sake of simplicity, the minimum energy pathways (which according to our calculations on coordination and pre-insertion intermediates are expected to be similar) are assumed identical, independently of the stereospecificity of the catalyst. However, the plots for the syndiospecific (Figure 9B) and isospecific (Figure 9C) models are different, since, as previously discussed, the enantioselectivities for the primary and secondary insertions

are in favor of the same or of opposite monomer enantiofaces, respectively.

In this framework, the lower regiospecificity of the isospecific catalytic systems can be rationalized by assuming that the activation energy for the rotation of the coordinated monomer around θ_0 between the orientations suitable for the primary and secondary insertions (schematically shown by dotted lines in Figure 9) is in general lower than (or comparable to) the activation energy for the secondary insertion.

For the syndiospecific model complexes, since their enantioselectivity is in favor of the same monomer enantioface for both primary and secondary insertions, when the coordination of the monomer with the wrong enantioface for the primary insertion occurs (situation b in Figures 5 and 9B), the most probable event is the dissociation of the coordinated monomer. It is also possible, with low probability, that the primary insertion of the wrong enantioface occurs, determining a stereoirregularity in the polymer chain. Secondary insertions with the wrong enantioface are expected to be essentially absent (see the high energy of situation e in Figures 5 and 9B). In the assumption of a low-energy barrier for the monomer rotation around θ_0, the regioselectivity would be simply determined by the differences between the activation energies for the secondary and primary insertions of the more suitable enantioface (and independent of the energy barrier for the monomer coordination). Moreover, the regiospecificity is expected to be high and similar to that of the corresponding aspecific catalytic complex.

For the isospecific model complexes, since their enantioselectivity is in favor of opposite monomer enantiofaces for primary and secondary insertions, when the coordination of the monomer with the enantioface unsuitable for the primary insertion occurs (situation b or e in Figures 7 and 9C), besides the dissociation of the coordinated monomer and besides a low probability of primary insertion (generating the stereoirregularities), also a low probability of secondary insertion (generating the regioirregularities) would be possible. This is due to the fact that the barrier for the dissociation of the coordinated monomer is not expected to be negligible with respect to the activation energy for the secondary insertion. Hence, for these isospecific model complexes, the amount of regioirregularities in the polymer chains would not be determined (as for the cases of aspecific and syndiospecific model complexes) by the differences between the activation energies for the secondary and primary insertions but would be related to the difference between the activation energies for the dissociation of the monomer (coordinated with the wrong enantioface) and the activation energy for its secondary insertion.

This dependence of the polypropene regioregularity on activation energies of different steps of the polymerization reaction, depending on the symmetry of the metallocene precursor (hence on its stereospecificity), is formally derived in the following.

For the case of the achiral catalytic complexes, with the assumption that the activation energy for the rotation of the coordinated monomer is in general lower than (or comparable to) the activation energy for the secondary insertion, the ratio between the rates of secondary and primary insertions can be approximated by:

$$\upsilon_s(C_{asp})/\upsilon_p(C_{asp}) \approx \exp[(\Delta E^{\ddagger}_p - \Delta E^{\ddagger}_s)/RT] \qquad (1)$$

where $\Delta E^{\ddagger}_p$ and $\Delta E^{\ddagger}_s$ are the activation energies for the primary and secondary insertions, respectively (see Figure 1A).

For the case of enantioselective catalytic complexes (isospecific and syndiospecific), let us call **r** and **w** the alkene-bound intermediates with chirality of monomer coordination *right* or *wrong* for the primary insertion (e.g., models A and B in Figure 6 or Figure 8, respectively). Moreover, let us indicate with M the propene monomer, with P, P_r, and P_w the alkene-free intermediates obtained after primary insertions from alkene-bound intermediates unspecified, **r**, and **w**, respectively, and with S_r and S_w the alkene-free intermediates obtained after secondary insertions from alkene bound intermediates **r** and **w**, respectively. Then, the main polymerization steps can be written:

$$\begin{aligned} P + M &\underset{k_{diss,r}}{\overset{k_{coord,r}}{\rightleftharpoons}} \mathbf{r} \overset{k_{p,r}}{\rightarrow} P_r \\ & \qquad\qquad\quad \mathbf{r} \overset{k_{s,r}}{\rightarrow} S_r \\ P + M &\underset{k_{diss,w}}{\overset{k_{coord,w}}{\rightleftharpoons}} \mathbf{w} \overset{k_{p,w}}{\rightarrow} P_w \\ & \qquad\qquad\quad \mathbf{w} \overset{k_{s,w}}{\rightarrow} S_w \end{aligned} \qquad (2)$$

where the activation energy for the rotation of the coordinated monomer between the orientations suitable for the primary and secondary insertions is assumed to be lower with respect to the activation energy for the secondary insertions.

In this framework, the rate of primary monomer insertion is:

$$\upsilon_p = \frac{dP_r}{dt} + \frac{dP_w}{dt} = k_{p,r}[\mathbf{r}] + k_{p,w}[\mathbf{w}] \qquad (3)$$

and the rate of secondary propene insertion is:

$$\upsilon_s = \frac{dS_r}{dt} + \frac{dS_w}{dt} = k_{s,r}[\mathbf{r}] + k_{s,w}[\mathbf{w}] \qquad (4)$$

The nonbonded energy calculations of the previous section suggest that, for the syndiospecific catalysts (C_s symmetric):

$$k_{s,r}[\mathbf{r}] \gg k_{s,w}[\mathbf{w}]$$

while for the isospecific catalysts (C_2 symmetric):

$$k_{s,r}[\mathbf{r}] \ll k_{s,w}[\mathbf{w}]$$

Hence, for the syndiospecific catalysts

$$\upsilon_s(C_{syn})/\upsilon_p(C_{syn}) \approx k_{s,r}[\mathbf{r}]/(k_{p,r}[\mathbf{r}] + k_{p,w}[\mathbf{w}]) \qquad (5)$$

moreover, let us assume for the sake of simplicity that the catalyst is highly enantioselective, then, $k_{p,r}[\mathbf{r}] \gg k_{p,w}[\mathbf{w}]$, and:

$$\upsilon_s(C_{syn})/\upsilon_p(C_{syn}) \approx k_{s,r}/k_{p,r} \approx \exp[(\Delta E^{\ddagger}_{p,r} - \Delta E^{\ddagger}_{s,r})/RT] \qquad (6)$$

that is, the amount of regioirregularities depends, as for the aspecific catalysts, on differences between the activation energies for the primary and secondary insertion steps, but for the enantioface that is right for the monomer insertion.

For the isospecific catalysts

$$\upsilon_s(C_{iso})/\upsilon_p(C_{iso}) \approx k_{s,w}[\mathbf{w}]/(k_{p,r}[\mathbf{r}] + k_{p,w}[\mathbf{w}]) \qquad (7)$$

If the approximation of the stationary state is applied to intermediates **r** and **w**:

$$k_{coord,r}[P][M] = k_{p,r}[\mathbf{r}] + k_{s,r}[\mathbf{r}] + k_{diss,r}[\mathbf{r}] \qquad (8)$$

$$k_{coord,w}[P][M] = k_{p,w}[\mathbf{w}] + k_{s,w}[\mathbf{w}] + k_{diss,w}[\mathbf{w}] \qquad (9)$$

then:

$$[\mathbf{r}] = k_{coord,r}[P][M]/(k_{p,r} + k_{s,r} + k_{diss,r}) \qquad (10)$$

$$[\mathbf{w}] = k_{coord,w}[P][M]/(k_{p,w} + k_{s,w} + k_{diss,w}) \qquad (11)$$

When the catalyst is substantially enantioselective, $k_{p,r}[\mathbf{r}] \gg k_{p,w}[\mathbf{w}]$, then eq 7 can be approximated by:

$$v_s(C_{iso})/v_p(C_{iso}) \approx k_{s,w}[\mathbf{w}]/k_{p,r}[\mathbf{r}] \quad (12)$$

and by substituting (10) and (11) in (12):

$$v_s(C_{iso})/v_p(C_{iso}) \approx$$
$$k_{s,w}k_{coord,w}(k_{p,r} + k_{s,r} + k_{diss,r})/k_{p,r}k_{coord,r}(k_{p,w} + k_{s,w} + k_{diss,w}) \quad (13)$$

For a catalyst which is substantially regioselective it can be also assumed that:

$$k_{p,r} \gg k_{s,r} + k_{diss,r}$$

then:

$$v_s(C_{iso})/v_p(C_{iso}) \approx$$
$$k_{s,w}k_{coord,w}/k_{coord,r}(k_{p,w} + k_{s,w} + k_{diss,w}) \quad (14)$$

Hence, in our framework, for the isospecific catalysts, the difference between the activation energies for secondary and primary insertions ($\Delta\Delta E^{\ddagger}_{reg}$) is expected to be dependent on the activation energies of several polymerization steps, also in the simplifying assumption of a high enantioselectivity.

Equation 14 can be simplified with the assumption that, for the monomer coordinated with the wrong enantioface, the activation energy for dissociation is much lower than the activation energy for its insertion ($k_{diss,w} \gg k_{p,w} + k_{s,w}$), then:

$$\Delta\Delta E^{\ddagger}_{reg}(C_{iso}) \approx$$
$$\Delta E^{\ddagger}_{s,w} + \Delta E^{\ddagger}_{coord,w} - \Delta E^{\ddagger}_{coord,r} - \Delta E^{\ddagger}_{diss,w} \quad (15)$$

According to our molecular mechanics analysis, $\Delta E^{\ddagger}_{coord,w} - \Delta E^{\ddagger}_{coord,r}$ can be approximated with $E_b - E_a$ of Figure 7 and hence is expected to be lower than 1 kcal/mol. As a consequence, the amount of regioirregularities would be mainly dependent on the difference between the activation energy for the dissociation of the monomer ($\Delta E^{\ddagger}_{diss,w}$) and the activation energy for its secondary insertion ($\Delta E^{\ddagger}_{s,w}$).

It is also worth noting that the activation energy for secondary monomer insertion starting from the alkene-free intermediate (see Figure 9C) is:

$$\overline{\Delta E}^{\ddagger}_{s,w} = \Delta E^{\ddagger}_{s,w} + \Delta E^{\ddagger}_{coord,w} - \Delta E^{\ddagger}_{diss,w} \quad (16)$$

hence:

$$\Delta\Delta E^{\ddagger}_{reg}(C_{iso}) \approx \overline{\Delta E}^{\ddagger}_{s,w} - \Delta E^{\ddagger}_{coord,r} \quad (17)$$

On the other hand, for the aspecific and syndiospecific catalysts, the corresponding $\Delta\Delta E^{\ddagger}_{reg}$ values (which are not available on the basis of our experimental results, since regioirregularities have not been detected) are expected to be simply:

$$\Delta\Delta E^{\ddagger}_{reg}(C_{asp}) \approx \Delta E^{\ddagger}_{s} - \Delta E^{\ddagger}_{p};$$
$$\Delta\Delta E^{\ddagger}_{reg}(C_{syn}) \approx \Delta E^{\ddagger}_{s,r} - \Delta E^{\ddagger}_{p,r} \quad (18)$$

Conclusions

In the course of our investigation of metallocene-catalyzed propene polymerization, we have found that achiral zirconocenes and hafnocenes, whether bridged or unbridged, substituted or unsubstituted, always produce atactic polypropenes with no detectable secondary units, not even as chain end groups. The high regiospecificity also has been confirmed for the syndiospecific zirconocene catalyst for the 0−70 °C polymerization temperature range, also for the less stereoregular fractions.

In the same polymerization conditions, the investigated isospecific zirconocenes produce isotactic polypropenes with substantial amounts of regioirregularities.

According to our calculations on model catalytic complexes, the lower regiospecificity of the isospecific catalytic systems with respect to the corresponding aspecific and syndiospecific systems would not be due to smaller differences between the activation energies for the minimum energy secondary and primary insertion paths, which would be instead similar.

In this respect, the only substantial difference between isospecific and syndiospecific model complexes is that the the low-energy pathways for the secondary and primary insertion correspond to **opposite** chiralities of coordination of the monomer for isospecific complexes, whereas they correspond to the **same** chirality of coordination of the monomer for syndiospecific complexes.

This difference accounts for the lower regiospecificity of the isospecific catalytic complexes, if the energy barrier for the rotation of the coordinated propene from the orientation suitable for the primary insertion (i.e., $\theta_0 \approx 0°$) toward an orientation suitable for the secondary insertion (i.e., $\theta_0 \approx 180°$) and vice versa are lower than the activation energy for the secondary insertion of the monomer.

In fact, for the isospecific models, the low-energy secondary insertion pathway (occurring for the propene enantioface unsuitable for the primary insertion) is only competing with the dissociation of the coordinated monomer and with the high-energy primary insertion (determining the stereoirregularities). On the contrary, for the syndiospecific as well as for the aspecific models, the low-energy secondary insertion path (occurring for the propene enantiofaces suitable for the primary insertion) is competing with the very low energy primary insertion pathway.

Acknowledgment. We thank F. Piemontesi for the microstructural analysis and M. Colonnesi for performing the polymerization experiments. Financial support from the "Ministero dell' Università e della Ricerca Scientifica e Tecnologica" and the "Progetto Strategico Chimica Fine" is gratefully acknowledged.

Appendix: Calculation Method

With respect to previous calculations[5] the molecular mechanics calculations presented in this paper are considerably less restrained, in fact, almost all the geometrical parameters have been relaxed. The only fixed parameters are those regarding the coordinated monomer molecule, for which, in the case of group 4 alkyl(alkene) metallocene cations, no reliable experimental data are available.

The calculations were performed with a package developed at the University of Naples. Energy minimizations were performed on internal coordinates. The BFGS algorithm[23] was used, and as convergence criterion we used 10^{-4} kcal/mol as the change of total energy and maximum gradients below the threshold of 10^{-3} kcal/(mol·Å) or kcal/(mol·deg) for bond distances and bend and torsion angles, respectively.

To prevent the effect of long-range attractive forces,[24] and as discussed in ref 24a, for the nonbonded interactions we assumed pure repulsive potentials according to the following

(23) (a) Broyden, C. G. *Math. Comput.* **1967**, *21*, 368. (b) Fletscher, R. *Comput. J.* **1970**, *13*, 371. (c) Goldfarb, D. *Math. Comput.* **1970**, *24*, 23. (d) Shanno, D. F. *Math. Comput.* **1970**, *24*, 647.

(24) Petraccone, V.; Pirozzi, B.; Frasci, A.; Corradini, P. *Eur. Polym. J.* **1976**, *12*, 323. (b) Sauers, R. R. *J. Chem. Educ.* **1996**, *73*, 114.

modified Lennard-Jones functional:

$$E_{nb} = \sum_{m<n}\left[\left(\frac{A_{ij}}{r_{mn}^{12}} - \frac{B_{ij}}{r_{mn}^{6}}\right) - \left(\frac{A_{ij}}{r_{ij}^{-12}} - \frac{B_{ij}}{r_{ij}^{-6}}\right)\right] \quad \text{for} \quad r_{mn} < \bar{r}_{ij}$$

$$E_{nb} = 0 \quad \text{for} \quad r_{mn} \geq \bar{r}_{ij}$$

where A_{ij}, B_{ij}, and $\bar{r}_{ij}$ are constants characteristic of species i and j and $\bar{r}_{ij}$ is the minimum interaction distance. Considering that the previous functional form has a discontinuity in the second derivative at $\bar{r}_{ij}$ and that this discontinuity causes an instability of the optimization algorithm, we preferred to fit an exponential function to the modified Lennard-Jones functional and use this exponential functional in the optimization processes.

The results presented in this paper are obtained within the scheme developed by Bosnich for bent metallocenes.[25] The approach used by Bosnich is a development of the CHARMM force field of Karplus[26] to include metallocenes of group 4A. In order to test the dependence of the results on the particular choice of parameters in the potential functions, some calculations were also performed by using the valence parameters of Bosnich−Karplus with the nonbonded parameters proposed by Scheraga and co-workers.[27] We also tested the approach proposed by Erker for the coordination of the carbon atoms of the π-ligand,[28] in conjunction with the AMBER force field of Kollman.[29] Although with the different sets of parameters the results are numerically different, the overall trends and the locations of the energy minima are nearly the same.

The same zero of the energy is adopted in the following for a given model complex, irrespective of the coordination chirality of the propene monomer.

Although crystalline structures of d^0 metal−olefin complexes, like those invoked as Ziegler−Natta catalytic intermediates, are now available,[30] it is difficult to assume a reliable distance Zr−C(olefin), which is however expected to be close to 2.5 Å. Hence, for the calculations presented in this paper, the distance Zr−C(olefin) was set equal to this value. Test calculations were repeated by varying this distance in the range 2.3−2.8 Å, obtaining qualitatively similar results.

The more complete energy optimizations with respect to previous works[5] (corresponding to a reduced rigidity of the bridged π-ligand) render the energy curves smoother and markedly reduce the energies for conformations far from the energy minima. However, the differences between the energy minima (corresponding to different diastereoisomeric intermediates) remain substantially unchanged. Although the numerical values of the energy differences depend also on the exact geometry and the energy parameters adopted in the calculations, no reasonable adjustment of these parameters seems to modify our conclusions.

JA964142Y

(25) Doman, T. N.; Hollis, T. K.; Bosnich, B. *J. Am. Chem. Soc.* **1995**, *117*, 1352.
(26) Brooks, B. R.; Bruccoleri, R. E.; Olafson, B. D.; States, D. J.; Swaminathan, S.; Karplus, M. *J. Comput. Chem.* **1983**, *4*, 187.
(27) Ooi, T.; Scott, R. A.; Vandekooi, K.; Scheraga, H. A. *J. Chem. Phys.* **1967**, *46*, 4410.
(28) Howeler, U.; Mohr, R.; Knickmeier, M.; Erker, G. *Organometallics* **1994**, *13*, 2380.
(29) Cornell, W. D.; Cieplak, P.; Bayly, C. I.; Gould, I. R.; Kenneth, M. M., Jr.; Ferguson, D. M.; Spellmeyer, D. C.; Fox, T.; Caldwell, J. W.; Kollman, P. A. *J. Am. Chem. Soc.* **1995**, *117*, 5179.
(30) Wu, Z.; Jordan, R. F. *J. Am. Chem. Soc.* **1995**, *117*, 5867.